Bio-Design and Manufacturing (2018) 1:195–202
https://doi.org/10.1007/s42242-018-0022-1

RESEARCH ARTICLE

Five-plane lancet needle design for soft PVC phantom tissue cutting

Yancheng Wang[1,2] · Deqing Mei[1,2]

Received: 8 July 2018 / Accepted: 12 August 2018 / Published online: 16 August 2018

Abstract

Lancet needle, having three planes at the tip to generate a sharp lancet point, is the most common needle tip geometry and used for medical procedures. This research presents two five-plane lancet needle designs, the five-plane lancet needle with two back bevels (FLN-B) and five-plane lancet needle with two front bevels (FLN-F), to study the effects of two additional bevel planes on the reduction of soft tissue cutting force. Mathematical models to calculate the inclination angle and rake angle along the cutting edges of FLN-B and FLN-F are developed. By using the grinding process, the prototype FLN-B and FLN-F needles are fabricated. And their inclination and rake angles along the cutting edges are investigated and compared to that of regular lancet needle. Needles insertion tests were conducted on soft PVC phantom which mimics the soft tissue. The initial peak insertion force and steady-state cutting force during needle insertion were identified, and the effect of cutting edge on needle soft tissue cutting force was studied. Compared to lancet needle, FLN-B and FLN-F both have higher inclination and rake angles at the tip cutting edge, could reduce the initial peak needle insertion force and tissue cutting forces, and thus can efficiently cut the soft tissue for medical applications.

Keywords Lancet needle · Needle insertion force · Rake angle · Inclination angle · Bevels · Five plane

List of symbols

λ	Inclination angle
α	Rake angle
F_c	Cutting force
F_{in}	Insertion force
F_{ex}	External friction force
γ	Radial coordinate to a point on the cutting edge
ξ	Bevel angle
φ	Secondary bevel angle
β	Angle of rotation
δ	Tertiary bevel angle
η	Secondary angle of rotation
$\gamma_d, \gamma_e, \gamma_g, \gamma_f$	Radial coordinate angles of points E, E, F, and G

✉ Yancheng Wang
yanchwang@zju.edu.cn

1 State Key Lab of Fluid Power and Mechatronic Systems, School of Mechanical Engineering, Zhejiang University, Hangzhou 310027, China

2 Key Laboratory of Advanced Manufacturing Technology of Zhejiang Province, School of Mechanical Engineering, Zhejiang University, Hangzhou 310027, China

Introduction

Needle is one of the most common features in medical devices [1, 2]. Needles are widely used in minimally invasive percutaneous procedures, such as injection, regional anesthesia, blood sampling, biopsy, brachytherapy. Lancet needle is the most commonly utilized hypodermic needle tip design, as shown in Fig. 1a. Two lancets generate a sharp point (P) at the tip to reduce the needle insertion force and the associated tissue deformation, needle deflection, and pain. Lancet needle is widely utilized in biopsy, vessel access, brachytherapy, drug injection, and other procedures. The tip geometry specification of lancet needle can be traced back to a US government GG-N-196 in 1946 [3]. For lancet needle, the cutting edge's geometry and grinding setup procedure and parameters have been studied [4]. Mathematical models to quantify the needle cutting edge inclination (λ) and rake (α) angles have been developed, and results demonstrated that two lancets at the needle tip can increase the λ and lower the needle insertion force [4]. Based on the model to estimate the initial peak needle insertion force [5, 6], optimal lancet needle geometry can be achieved, which has large lancets on the tip and could reduce the needle insertion force by 14% [7].

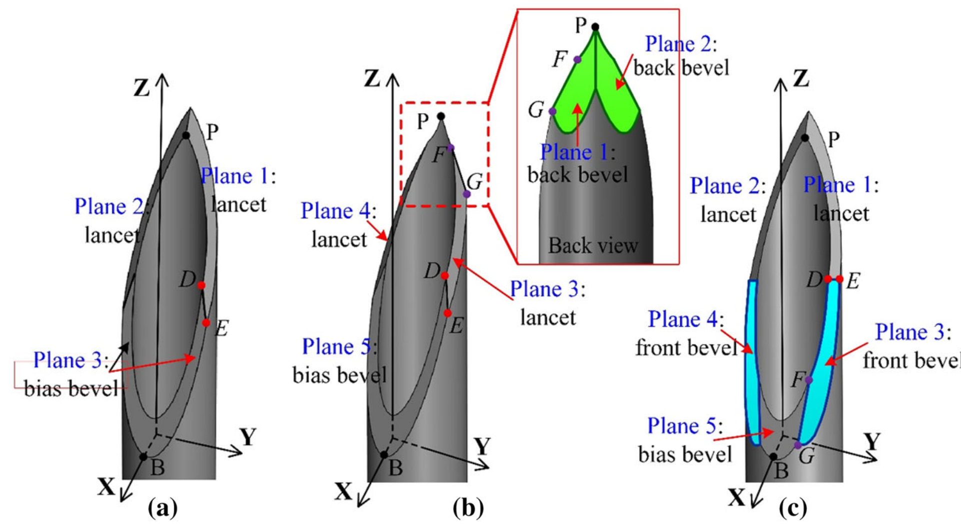

Fig. 1 **a** Regular lancet needle and five-plane lancet needles: **b** FLN-B and **c** FLN-F [25]

Along the needle tip cutting edge, two parameters, the λ and α, have demonstrated to be critical for the needle insertion force [5, 8]. The concept of increasing the λ along the needle cutting edge to reduce the needle insertion force has been demonstrated [4, 6]. For example, either grinding two back bevels [9] or two front lancets [4, 10–12] to generate a three-plane needle can lower the needle insertion force over the single-plane bias bevel needle. To advance the current three-plane NLP, grinding two more bevel planes either on the back (FLN-B in Fig. 1b) or on the front (FLN-F in Fig. 1c) to create the five-plane needles is expected to reduce the needle insertion force. In FLN-B, grinding two back bevels (Planes 1 and 2) can sharpen the tip at lancet point P, as in Fig. 1b. In FLN-F, grinding two additional front bevels (Planes 3 and 4) on the bias bevel section, the cutting edges transition from the lancets (Planes 1 and 2) to remaining bias bevel (Plane 5) become smooth and sharper. Recently, FLN-F has been proposed to reduce the needle insertion force [13] and utilized for diabetic patients [14] or general needle injection [15, 16]. However, these studies have not quantified the λ and α of these new needle designs and become one goal of this research.

Insertion force and bevel length are two key criteria to evaluate the performance of a needle tip design. Grinding two more planes has minimal and no effect on the bevel length for FLN-B and FLN-F, as shown in Fig. 1b, c, respectively. For hollow needle insertion, the axial insertion force can be divided into three components: the cutting force (F_c), inner friction force (F_{in}) between tissue sample and needle inside surface, and outer friction force (F_{ex}) between tissue and needle outside surface. To characterize the needle soft tissue cutting efficiency, the cutting force needs to be decomposed from the axial insertion force. For solid needle, Abolhassani et al. [17] and Kobayashi et al. [18] measured the needle insertion force when the tip was out of the tissue and regarded this force as the external friction force (F_{ex}) to find the cutting force (F_c). Howard et al. [19] and Winine et al. [20] used an approach to insert the same needle into tissue twice at the same location to find the F_c and F_{ex}. For hollow needle insertion, Li and Wang [21] developed an approach of using double needle insertion into several tissue samples with different lengths to decompose the F_c, F_{in}, and F_{ex} and found F_{ex} contributes a large proportion in total insertion force. Therefore, the effects of F_{ex} need to be eliminated in order to investigate the effects of needle cutting edge on soft tissue cutting performances. To simplify the experiment procedure, we followed the double needle insertion method described in [21] to eliminate the effect of F_{ex} and study the effect of the cutting edges of FLN-B and FLN-F on tissue cutting force.

In this paper, the geometry and mathematical models to calculate λ and α for FLN-B and FLN-F are presented. Then, the prototype FLN-B and FLN-F needles are fabricated. The λ and α for the ground FLN-B and FLN-F needles are studied and compared to regular lancet needle. This is followed by needle insertion experiments. PVC phantom is used to mimic soft tissue, and the results are discussed. Finally, the conclusions and future works are presented.

Five-plane lancet needle design

Needles are usually fabricated by a burr-free grinding process. The geometry of lancet needle is determined by three grinding parameters: bevel angle (ξ), secondary bevel angle (φ), and angle of rotation (β) [4]. As in Fig. 1a, grinding two lancets divides the needle tip into two sections. From the tip, Section 1 is two lancets at the tip and Section 2 is the remaining bias bevel plane. A line DE is the intersection between the lancet and bias bevel planes. To characterize lancet needle cutting edge, the equations to calculate the λ and α for lancet needle have been derived in [4]. In Section 2, the λ and α for remaining bias bevel cutting edges are [4]

$$\lambda = \arcsin \frac{|\cot \xi \sin \gamma|}{\sqrt{1 + \cot^2 \xi \sin^2 \gamma}} \tag{1a}$$

$$\alpha = \arccos \sqrt{\cos^2 \gamma \sin^2 \xi + \sin^2 \gamma} \tag{1b}$$

where γ is the radial coordinate to a point on the cutting edge. An xyz coordinate axis is defined for the needle by the z-axis coinciding with the needle axis and the x-axis passing through the lowest point of the needle tip profile.

In Section 1, the λ and α for lancets' cutting edges are [4]

$$\lambda = \arcsin \frac{|\cot \varphi \sin(\gamma \pm \beta)|}{\sqrt{1 + \cot^2 \varphi \sin^2(\gamma \pm \beta)}} \tag{2a}$$

$$\alpha = \arccos \sqrt{\cos^2(\gamma \pm \beta) \sin^2 \varphi + \sin^2(\gamma \pm \beta)} \tag{2b}$$

FLN-B

For FLN-B as shown in Fig. 2a, besides three angles: ξ, φ, and β, two additional angles, tertiary bevel angle (δ) and secondary angle of rotation (η), are used to grind two back bevels at regular lancet needle tip. These two back bevels and lancets divide the needle tip into three sections. From the tip, Section 1 is the back bevels, Section 2 is the remaining two lancets, and Section 3 is the remaining bias bevel. Typically, grinding two back bevels only affect the lancets section and maintains the same bias bevel as lancet needle, as shown in Fig. 2a. The cutting edges on Sections 1, 2, and 3 are marked by the azure, green, and blue lines, respectively, as shown in Fig. 2b, d.

In Sections 2 and 3, formulas for λ and α for remaining lancets and bias bevel's cutting edges are the same as lancet needle. Equations (1a)–(1b) and (2a)–(2b) can be used to calculate the λ and α for remaining bias bevel and lancets' cutting edges, respectively. In Section 1, there have two parts: curved line PF and line FG between the back bevels and lancets [22]. The λ and α for the curved line PF' cutting edges are

$$\lambda = \arcsin \frac{|\cot(\delta) \sin(\gamma \pm \eta + \pi)|}{\sqrt{1 + \cot^2 \delta \sin^2(\gamma \pm \eta + \pi)}} \tag{3a}$$

$$\alpha = \arccos \sqrt{\cos^2(\gamma \pm \eta + \pi) \sin^2 \delta + \sin^2(\gamma \pm \eta + \pi)} \tag{3b}$$

Line FG is the cross-product of the normal vector ($\boldsymbol{n}_1$) of the lancet surface and normal vector ($\boldsymbol{n}_2$) of the back bevel plane. To define the λ and α on the line FG in Section 1's cutting edge, three vectors $\boldsymbol{s}$, $\boldsymbol{v}$, and $\boldsymbol{c}$, are defined at a point A on the needle cutting edge: $\boldsymbol{s}$ is tangent to the cutting edge and is the cross-product of the normal vectors $\boldsymbol{n}_1$ and $\boldsymbol{n}_2$, $\boldsymbol{v} = \{0, 0, 1\}$ is along the cutting direction, and $\boldsymbol{c}$ is the projection of vector $\boldsymbol{s}$ in plane P_r and perpendicular to the $\boldsymbol{v}$. The λ is defined as the angle between vectors $\boldsymbol{s}$ and $\boldsymbol{c}$. The α is the angle between two vectors $\boldsymbol{a}$ and $\boldsymbol{b}$, where $\boldsymbol{a}$ is the intersection between planes $\mathrm{P_n}$ and A_γ and $\boldsymbol{b}$ is the intersection of planes P_n and P_r. Plane P_n is normal to the cutting edge and has a normal vector of $\boldsymbol{s}$. The normal vectors $\boldsymbol{n}_1$ (lancet) and $\boldsymbol{n}_2$ (back bevel) can be expressed as

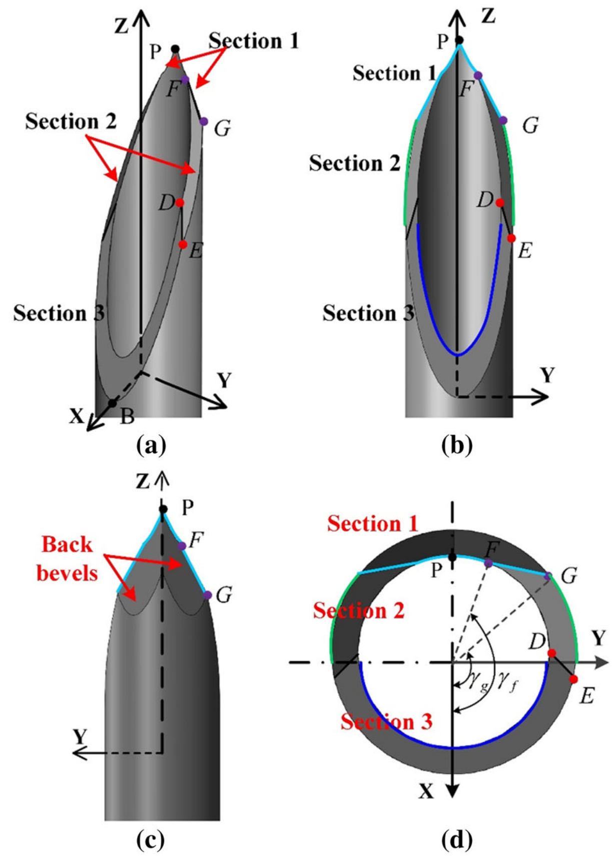

Fig. 2 FLN-B needle: **a** isometric, **b** front, **c** back, and **d** top views

$$\boldsymbol{n}_1 = \{\cos \beta \cos \varphi, -\sin \beta \cos \varphi, \sin \varphi\} \tag{4a}$$

$$\boldsymbol{n}_2 = \{\cos \eta \cos \delta, -\cos \delta \sin \eta, \sin \delta\} \tag{4b}$$

Thus, the vectors $\boldsymbol{s}$, $\boldsymbol{a}$, and $\boldsymbol{b}$ can be calculated as

$$\boldsymbol{s} = \{-\sin \beta \cot \varphi + \sin \eta \cot \delta, \cos \eta \cot \delta - \cos \beta \cot \varphi, \cot \varphi \cot \delta (\sin \beta \cos \eta - \cos \beta \sin \eta)\} \tag{5a}$$

$$\boldsymbol{a} = \boldsymbol{s} \times \boldsymbol{n}_1 = \{\sin \xi (\cos \varphi - 1), \sin \varphi (\cot \xi \cos \xi + \sin \xi), \cos \xi (1 - \cos \varphi)\} \tag{5b}$$

$$\boldsymbol{b} = \boldsymbol{s} \times \boldsymbol{v} = \{\cos \eta \cot \delta - \cos \beta \cot \varphi, \sin \beta \cot \varphi - \sin \eta \cot \delta, 0\} \tag{5c}$$

Thus, the formulas to calculate λ and α on cutting edge FG can be derived as

$$\lambda = \arcsin \frac{|\boldsymbol{s} \cdot \boldsymbol{v}|}{\|\boldsymbol{s}\|\|\boldsymbol{v}\|} \tag{6a}$$

$$\alpha = \arccos \frac{\boldsymbol{a} \cdot \boldsymbol{b}}{\|\boldsymbol{a}\|\|\boldsymbol{b}\|} \tag{6b}$$

The locations of points D, E, F, and G determine the transition position between Sections 1, 2, and 4, respectively. As in Fig. 2d, the radial coordinate $\gamma_{\text{d}}, \gamma_{\text{e}}, \gamma_{\text{g}}, \gamma_{\text{f}}$, can be calculated as

$$\gamma_{\text{d}} = \arccos\left(\frac{1 - \csc^2\beta(\cos\beta - \cot\xi\tan\varphi)^2}{\csc^2\beta(\cos\beta - \cot\xi\tan\varphi)^2 + 1}\right) \tag{7a}$$

$$\gamma_{\text{e}} = \arccos\left(\frac{-m_{\text{DE}}^2 r_i + \sqrt{r_o^2 + m_{\text{DE}}^2(r_o^2 - r_i^2)}}{(1 + m_{\text{DE}}^2)r_o}\right) \tag{7b}$$

$$\gamma_{\text{f}} = \arccos\left(\frac{1 - m_{\text{FG}}^2}{1 + m_{\text{FG}}^2}\right) \tag{7c}$$

$$\gamma_{\text{g}} = \arccos\left(\frac{-m_{\text{FG}}^2 r_i + \sqrt{r_o^2 + m_{\text{FG}}^2(r_o^2 - r_i^2)}}{(1 + m_{\text{FG}}^2)r_o}\right) \tag{7d}$$

where $m_{\text{DE}} = \frac{\cos\beta - \cot\xi\tan\varphi}{\sin\beta}$ and $m_{\text{FG}} = \frac{\cos\eta\cot\delta - \cot\beta\cot\varphi}{\sin\eta\cot\delta - \sin\beta\cot\varphi}$ are the slopes of line DE and ling FG on XY plane, respectively.

FLN-F

As in Fig. 3a, FLN-F needle tip design is to ground two extra bevels on the front remaining bias bevel surface, which can enhance the needle tip performance. The geometry of FLN-F needle is determined by five grinding parameters: bevel angle (ξ), secondary bevel angle (φ), and angle of rotation (β), tertiary bevel angle (δ), and secondary angle of rotation (η). These two extra bevels and lancets divide the needle tip into three sections: Section 1 is the two lancets the same as NLP needle, Section 2 is the additional bevels, and Section 3 is the remaining bias bevel. Lines DE and FG are the intersections between Sections 1 and 2 and Sections 2 and 3, respectively. In Fig. 3a, the cutting edges on Sections 1, 2, and 3 are marked by the green, azure, and blue lines, respectively.

In Sections 1 and 3, the λ and α for lancets and remaining bias bevel's cutting edges are the same as lancet needle. In Section 2, the cutting edges are the intersections between two ground extra bevels and bias bevel. Thus, the λ and α for Section 3's cutting edge are:

$$\lambda = \arcsin \frac{|\cot\delta\sin(\gamma \pm \eta)|}{\sqrt{1 + \cot^2\delta\sin^2(\gamma \pm \eta)}} \tag{8a}$$

$$\alpha = \arccos\sqrt{\cos^2(\gamma \pm \eta)\sin^2\delta + \sin^2(\gamma \pm \eta)} \tag{8b}$$

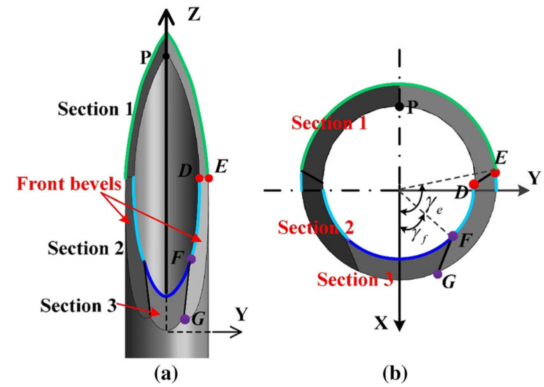

Fig. 3 FLN-F needle: **a** front and **b** top views

The locations of points E and F determine the initial transition between Sections 1, 2, and 3, respectively. For FLN-F, Section 1 occurs when $\gamma_{\text{e}} \le \gamma \le 360° - \gamma_{\text{e}}$, Section 2 occurs when $\gamma_{\text{f}} \le \gamma \le \gamma_{\text{e}}$ and $360° - \gamma_{\text{e}} \le \gamma \le 360° - \gamma_{\text{f}}$, Section 3 occurs when $0 \le \gamma \le \gamma_{\text{f}}$ and $360° - \gamma_{\text{f}} \le \gamma \le 360°$.

Protype FLN-B and FLN-F needles

FLN-B and FLN-F needles fabrication

To study the performance of the proposed five-plane lancet needle, a FLN-B and a FLN-F are ground by using the using the needle grinding setup outlined in [4] and procedures and parameters presented in [25]. For the baseline NLP, a commercial lancet needle (Becton–Dickinson) is selected. By using the reverse engineering method [7], the baseline lancet needle, with $\xi = 15°$, $\varphi = 20°$, and $\beta = 60°$, is also ground. Figure 4 shows the final fabricated results of FLN-B, FLN-F, and regular NLP needles. The FLN-B and FLN-F have the same setup parameters: $\xi = 15°$, $\varphi = 20°$, $\beta = 60°$, $\delta = 10°$, and $\eta = 30°$. In Fig. 4, the FLN-B has the same bias bevel section as the lancet needle, while the FLN-F has almost the same lancets section as lancet needle. These needles are 11 gauge thin wall 316 stainless steel needles (OD 3.05 mm and ID 2.54 mm).

Inclination and rake angles of FLN-B and FLN-F

For lancet needle (NLP), ranges of inclination and rake angles are $0 \le \lambda \le 90° - \varphi$ and $0 \le \alpha \le 90° - \varphi$, as shown in Fig. 5. The maximum λ ($= 90° - \varphi = 70°$) occurs at $\gamma = 150°$ and 210°. The locations of $\gamma = 150°$ and 210° are determined by the angle of rotation $\beta = 60°$, which shifts the location of the maximum λ from $\gamma = 90°$ and 270° for the single-plane bias bevel needle to $\gamma = 150°$ and 210° for these lancets. At $\gamma =$ 180°, where the needle tip first contacts the tissue, $\lambda = 67.2°$, much higher than that of single-plane bias bevel needle ($\lambda =$

Needle number	Regular NLP	FLN-F (with two front bevels)	FLN-B (with two back bevels)
Needles	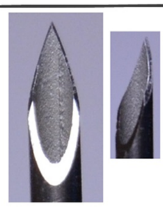	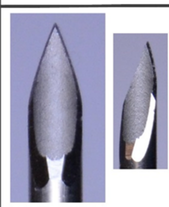	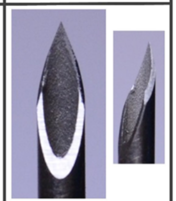
Angles	$\xi = 15°$ $\varphi = 20°$ $\beta = 60°$	$\xi = 15°$ $\varphi = 20°$ $\beta = 60°$ $\delta = 10°$ $\eta = 30°$	$\xi = 15°$ $\varphi = 20°$ $\beta = 60°$ $\delta = 10°$ $\eta = 30°$

Fig. 4 Ground FLN-B, FLN-F, and regular NLP needle tips

0°) and demonstrated the concept of grinding two lancets on the tip can sharpen and increase the λ at the needle tip [4]. For the rake angle, the maximum α (=75°) occurs at $\gamma = 0°$ and 180°. The higher rake angle also represents a sharper cutting edge and have demonstrated beneficial for steady-state soft tissue cutting after fracture [23]. In Section 1, the minimum α (=0°) occurs at $\gamma = 150°$ and 210°.

For FLN-B, in Section 1, the maximum λ is 77.5° at $\gamma = 157.3°$ and 202.7°, the transition from the curved line PF to intersection line FG. At point P ($\gamma = 180°$), λ is 70.6°, higher than that of NLP, as shown in Fig. 5. At the transition line FG, from $\gamma = 128.8°$ to 157.3° and 202.7° to 231.2° (between the back bevels and lancets), the λ has a constant value of 65.4°. In Section 2 (remaining lancets) and 3 (bias bevel), λ is the same as that of NLP. For the rake angle, in the back bevel section, the α is greatly increased compared to NLP. At the lancet point P ($\gamma = 180°$), the α is increased to 58.5° (from 28.0° in NLP). The minimum α (=0°) occurs at $\gamma = 90°$ and 270°, where are the transition between the bias bevel and lancets section, the same as that in NLP. In Section 2, the cutting edge created by bias bevel grinding has the same λ and α as NLP.

As for FLN-F, in Section 1, the cutting edge created by grinding two lancets has the same λ and α as the NLP. The λ at point P ($\gamma = 180°$) is 67.2°. In Section 2, the maximum λ (=79.1°) occurs at $\gamma = 96.3°$ and 263.7°, the transition angles of Section 1 (lancets) and 2 (extra front bevel). The maximum λ = 79.1° is higher than the maximum λ in NLP and FLN-B. In Section 3 (bias bevel), the same λ and α as the NLP are observed. For the rake angle, the same trends are observed. The α in Section 2 is much higher than that of NLP, and maximum $\alpha = 71.4°$ occurs at $\gamma = 45.7°$ and 314.3°, which is the transition angle of the Section 2 (extra front bevel) and 3 (bias bevel), as shown in Fig. 5.

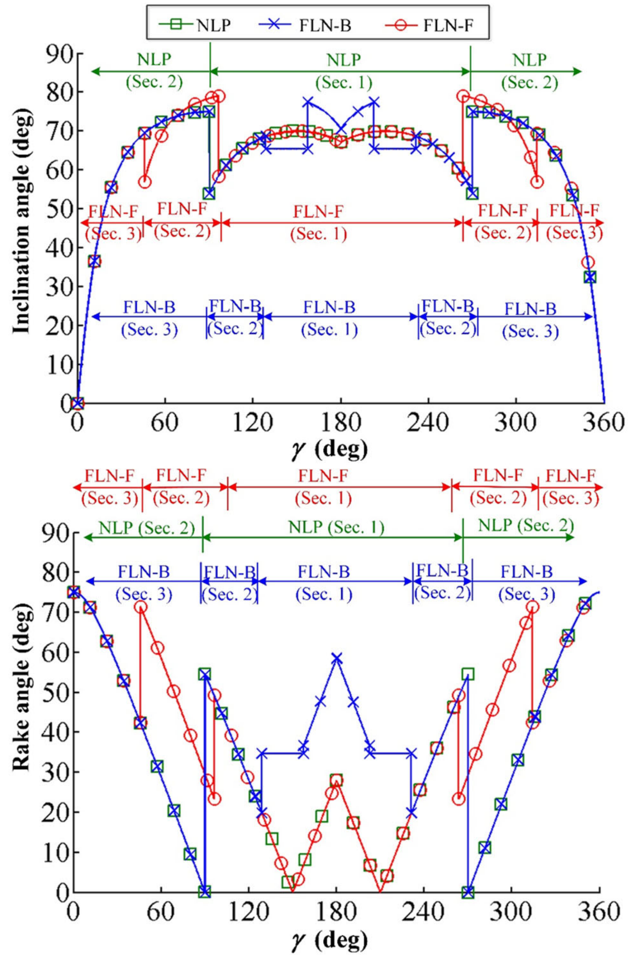

Fig. 5 λ and α of FLN-B, FLN-F, and regular NLP [25]

Overall, FLN-B and FLN-F tips have higher inclination and rake angles than that of NLP.

PVC phantom tissue cutting

Needle insertion experiment

The overview of the experimental setup to perform the needle insertion test is shown in Fig. 6. Three linear stages (Siskiyou Model 200 cri and 100 cri, Grants Pass, Oregon) were assembled to insert the needle into the polyvinyl chloride (PVC) phantom tissue [25]. The PVC phantom was produced from a mixture of 1:1 ratio of regular liquid plastic to plastic softener and was selected to mimic the soft tissue due to its homogenous properties [24]. The tissue indentation test showed that the PVC phantom has a Young's modulus of 12.4 kPa. The phantom tissue was constrained in a tissue holder, which is used to mold the phantom. The needle was secured on a needle holder, which attached on a linear stage. During the experiment, the needle will be driven by the linear stages to insert into the phantom tissue.

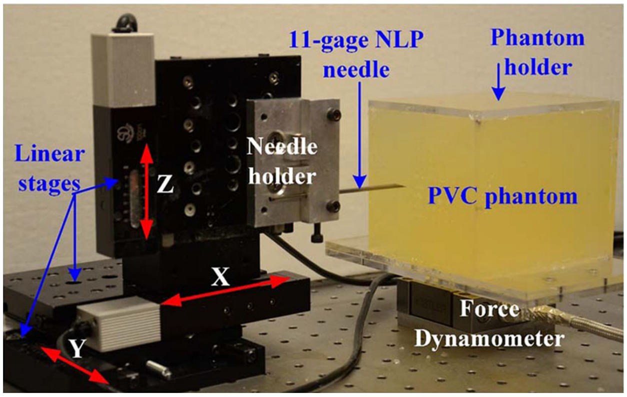

Fig. 6 Experimental setup for needle insertion test

During the experiment, three needles shown in Fig. 4 are inserted into the PVC phantom tissue. Each needle was inserted 30 mm into the tissue at a constant speed of 1.5 mm/s and controlled by the linear stages. To measure the needle insertion force, a Kistler 9256C piezoelectric force dynamometer (Winterthur, Switzerland) with an accuracy of 0.002 N and linearity lower than 0.04% full scale output was placed underneath the tissue holder. For each needle, three repeated tests for each needle were conducted.

It is known that the insertion force consists of cutting force and friction force. Friction force is contributed from the outer and inner surfaces of needle. To extract the cutting force, two repeated needle insertions were conducted. In the first needle insertion, the measured insertion force is the combination of friction and cutting forces. In second needle insertion, the measured insertion force is predominately by the friction force because the needle travels through the hole made in first insertion without new tissue cutting. The subtraction of two measured forces can be seen as the cutting force.

Needle tissue cutting force

Figure 7 shows the measured needle insertion forces versus time for regular lancet, FLN-B, and FLN-F needles while insertion into the PVC phantom. In first needle insertion force profile, there has three districted phases. Phase 1 is the deformation phase where the PVC phantom deflects and the force increases with no tissue cutting. Phase I ends at the initial peak needle insertion force (F_N), which is defined at the transition between Phases I and II. Phase II is defined by observing the slop change after the needle cutting edge completely entered the phantom tissue. Phase III is the steady-state cutting phase [21, 23], and all the cutting edges are involved into soft tissue cutting. In this phase, the needle insertion force is the sum of needle tip cutting force and friction force along the needle tip and shaft. In second needle insertion along the same insertion path, only friction force was generated outside the needle shaft without new tissue cutting. In Fig. 7, we can see that the friction force takes a majority portion of needle insertion force. Also, as the increase in needle insertion distance, the friction force is also increased. As for needle cutting force, it can be defined as the discrepancy between the first and second needle insertion forces in the steady-state cutting phase [23]. To reduce the friction force, two methods can be utilized. The first is using the surface finishing process to polish the needle surface with the aim to achieve a better surface finishing of needles and in turn to reduce the friction force. The second is to texture the micro-patterned surfaces on needle shaft and to reduce the friction force. In Fig. 7, we can see that the cutting fore in the last 5 mm of needle insertion reaches a more steady-state level. Thus, in this study, we utilized the average cutting force in the last 5 mm needle insertion to present the steady-state tissue cutting force. As in Fig. 7, the steady-state cutting forces for regular lancet, FLN-B, and FLN-F needles are 0.24 N, 0.19 N, 0.12 N, respectively.

Besides steady-state cutting force, initial peak needle insertion force (F_N) has been utilized to study the needle insertion performance. The F_N is required to initially fracture the tissue bonds and begin penetration [5, 7, 24]. As in Fig. 7, the F_N for regular lancet, FLN-B, and FLN-F needles are 0.38 N, 0.22 N, and 0.23 N, respectively. FLN-B and FLN-F needles have a much lower initial peak needle insertion force and shorter deformation phase to rupture the tissue bonds and initiate tissue cutting over regular lancet needles.

Figure 8 shows the average and standard deviation of three measured F_N and steady-state cutting force for these three types of needles. The average of measured F_N for FLN-B (0.32 N) and FLN-F (0.31 N) is relatively lower than that of regular lancet needle (0.36 N). The cutting forces for LN-B and FLN-F are 0.19 N and 0.15 N, respectively, about 82.6% and 65.2% of regular lancet needle. Such noticeable difference between the F_N and cutting force of these three needles could be attributed to the effect of needle tip cutting edge geometry.

Discussion

The needle cutting edge can be characterized by α and λ, which have been demonstrated to be important for the needle insertion force. Prior studies showed that the needle with higher λ can lower F_N for needle insertion [21, 23]. This observation can be applied to the results shown in Fig. 8. The λ for regular lancet (NLP), FLN-B, and FLN-F needles are shown in Fig. 5. At initial peak needle insertion force point, the lancet section's cutting edge is critical, due to the contact area between the needle and tissue mainly concentrated on the lancet section at the moment of initial tissue cutting. For FLN-B, two back bevels grinding sharpen the tip, which increases the λ on the tip back bevel section. The

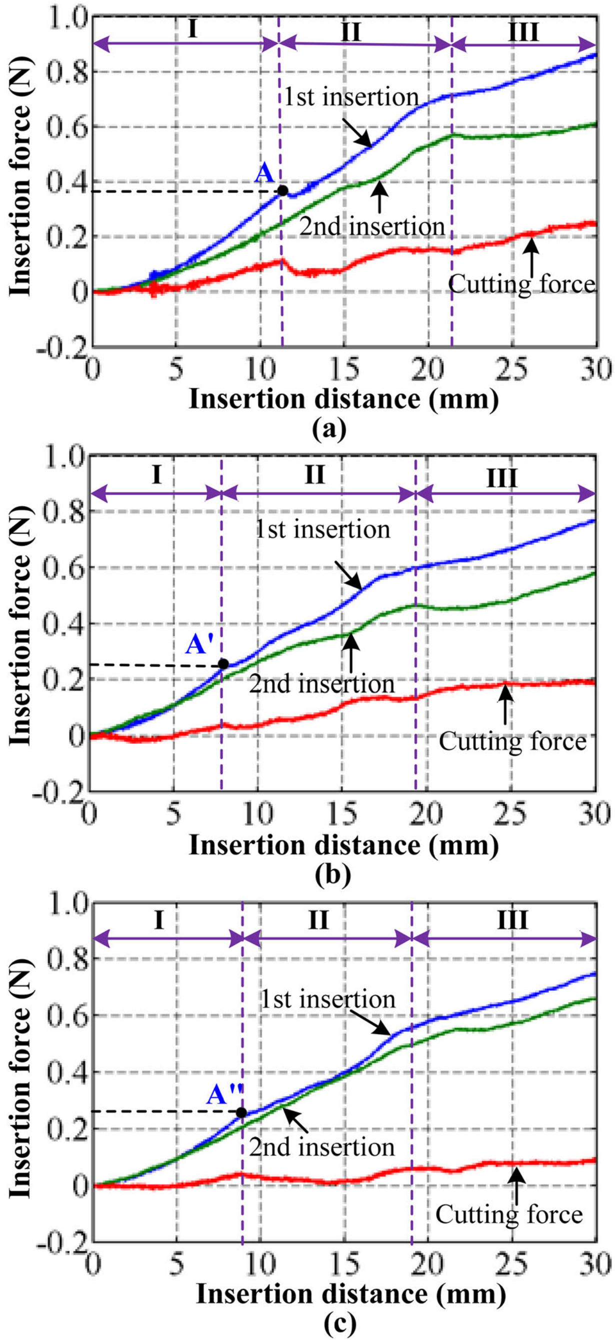

Fig. 7 Needle insertion forces: **a** regular lancet, **b** FLN-B, and **c** FLN-F needles

maximum λ is 77.5° at $\gamma = 157.3°$ and 202.7°; and at $\gamma = 180°$, λ is 70.6°, still higher than that of lancet needle. Thus, it leads to a lower force (about 0.33 N), about 8.3% reduction over the NLP (0.36 N). For FLN-F, it has the same tip geometry in lancet section as regular lancet needle (as shown in Fig. 5), but the geometry of remaining bias bevel section (as in Fig. 4) leads to a smaller wedging actions of the needle tip reduce the needle insertion force.

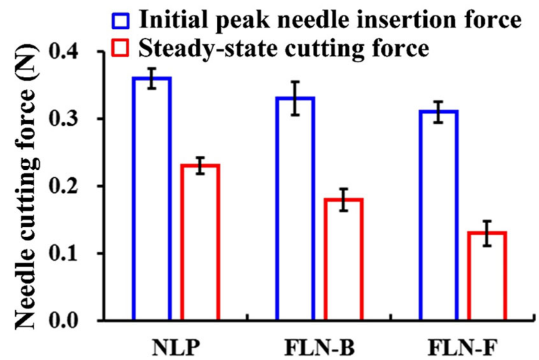

Fig. 8 Needle cutting force for the NLP, FLN-B, and FLN-F needles

For the steady-state cutting phase, the rake angle (α) becomes more dominant than the inclination angle (λ) on the cutting force. Overall, FLN-B and FLN-F tips have higher rake angle than that of lancet needle, as shown in Fig. 5. It confirms that the needle with large rake can reduce the cutting force during needle soft tissue insertion. FLN-B has the highest rake angle (58.5°) at the tip point, and it reduces the cutting force by 17.4% over lancet needle. As for the comparison of FLN-B and FLN-F needles, FLN-F needle has better performances, and it can reduce the initial peak insertion force by 13.8% and lower the cutting force by 34.8%. The reasons can be explained as: FLN-F needle has larger length of two front bevels than that of FLN-B needle with two back bevels. They could be used for enhanced soft tissue cutting to lower tissue cutting force. Furthermore, in Fig. 5, we can see that the region of two front bevels in FLN-F has the highest rake angles than that of FLN-B. Thus, FLN-F with greater rake angle in the region of two front bevels can cut the soft tissue more efficiency and generate lowest tissue cutting force. Results obtained in this study demonstrated that the needle with multiple bevels ground at the tip tends to sharpen the needle tip and reduce the cutting force during soft tissue insertion. To obtain the real needle insertion characteristics of these three types of needles, animal tissue tests (including muscle, fat, skin, and liver) will be conducted in future work.

Conclusions

This study presented two five-plane lancet needle designs, FLN-B and FLN-F, to sharpen the needle tip cutting edge and reduce the soft tissue cutting force. The mathematical models to calculate the inclination and rake angle of the FLN-B and FLN-F are derived. Compared to lancet needle, FLN-B and FLN-F both had higher inclination and rake angles at the needle tip which were beneficial for efficient soft tissue cutting. PVC phantom tissue cutting experiments demonstrated that the FLN-B and FLN-F can reduce the initial peak insertion forces by 11.1% and 13.8%, respectively. By using double needle insertion tests, the tissue cutting force can be extracted from the total needle insertion force. Compared to regular lancet needle, results showed that the FLN-B and FLN-F could lower the tissue cutting force by 17.4% and 34.8%, respectively.

The mathematical model developed in this study opens the opportunity to design advanced hypodermic needle tip to minimize the needle insertion force. Especially, optimal five-plane lancet needle tip geometry design will be conducted in future work. Further, applications of the five-plane lancet needles in medical procedures will also be conducted.

Acknowledgements The research is funded by the Scientific Research Foundation for the Returned Overseas Chinese Scholars (No. 2014 1685), and Open Fund of Shanghai Key Laboratory of Digital Manufacture for Thin-walled Structures. We also want to thank Prof. Bruce Tai from Texas A&M University, Prof. Roland Chen from Washington State University, Prof. Albert Shih from University of Michigan for their help on five-plane needles' design and grinding.

References

1. Kucklick T (2006) The medical device R&D handbook. Taylor & Franics, Boca Raton
2. Wang YC, Li WS, Han PD, Giovannini M, Ehmann K, Shih A (2016) Contributions in medical needle technologies- geometry, mechanics, design and manufacturing. Mach Sci Technol 20(1):1–43
3. DIN 13097-4: 2009-08 (2009) Hypodermic needles—part 4: point geometry, requirement and testing, Standard
4. Wang YC, Tai BL, Chen RK, Shih AJ (2013) The needle with lancet point-geometry for tip grinding and tissue insertion force. ASME J Manuf Sci Eng 135:041010–041017
5. Moore JZ, Malukhin K, Shih AJ, Ehmann KF (2011) Hollow needle tissue insertion force model. CIRP Ann Manuf Technol 60:157–160
6. Moore JZ, McLaughlin PW, Shih AJ (2012) Novel needle cutting edge geometry for end-cut biopsy. Med Phys 39:99–108
7. Wang YC, Chen RK, Tai BL, Shih AJ (2014) Optimal needle design for minimal insertion force and bevel length. Med Eng Phys 36:1093–1100
8. Moore JZ, Zhang QH, McGill CS, Zheng HJ, McLaughlin PW, Shih AJ (2010) Modeling of the plane needle cutting edge rake and inclination angles for biopsy. ASME J Manuf Sci Eng 132:051005-1–051005-8
9. Das S, Ghatak A (2011) Puncturing of soft gels with multi-tip needles. J Mater Sci 46:2895–2904
10. Busillo E, Colton JS (2009) Characterization of plastic hypodermic needles. ASME J Med Dev 3:041004–041009
11. Ross CF (2004) Hypodermic needle. US patent 6702790, 9 Mar
12. Gravlee JF (1998) Hypodermic needle. US patent 5733266, 31 Mar
13. Doyle JL, Koziol SL (2000) Five beveled point geometry for a hyperdermic needle. US Patent 6009933, 4 Jan
14. Hiesch L, Gibney M, Berube J, Manocchio J (2012) Impact of a modified needle tip geometry on penetration force as well as acceptability, preference, and perceived pain in subjects with diabetes. J Diabetes Sci Technol 6(2):328–335
15. Jaber A, Bozzato GB, Vedrine L, Prais WA, Berube J, Laurent PE (2008) A novel needle for subcutaneous injection of interferon beta-1a: effect on pain in volunteers and satisfaction in patients with multiple sclerosis. BMC Neurol 8:12–38
16. Vedrine L, Prais W, Laurent PE, Raynal-Olive C (2003) Improving needle-point sharpness in prefillable syringes. Med Dev Technol 14(4):32–35
17. Abolhassani N, Patel R, Moallen M (2007) Needle insertion into soft tissue: a survey. Med Eng Phys 29(4):413–431
18. Kobayashi Y, Sato T, Fujie MG (2009) Modeling of friction force based on relative velocity between liver tissue and needle for needle insertion simulation. In: 31st Annual international conference of the IEEE EMBS, pp 5274–5278
19. Howard MA, Abkes BA, Ollendieck MC, Noh MD, Ritter RC, Gillies GT (1999) Measurement of the force required to move a neurosurgical probe through in vivo human brain tissue. IEEE Trans Biomed Eng 46(7):891–894
20. Winnie J, Yoshida K, Hofinann UG (2007) In vivo implant mechanics of single-shaft microelectrodes in peripheral nervous tissue. In: Proceedings of the 3rd international IEEE EMBS conference on neural engineering, vol 07, pp 1–4
21. Li WS, Wang YC, Nteziyaremye C, Yamaguchi H, Shih AJ (2016) Measurement of the friction force inside the needle in biopsy. ASME J Manuf Sci Eng 138:031003–031008
22. Han PD, Che DM, Pallav K, Ehmann K (2012) Models of the cutting edge geometry of medical needles with applications to needle design. Int J Mech Sci 65:157–167
23. Tai BL, Wang YC, Shih AJ (2013) Cutting force in hollow needle insertion of soft tissue. In: 2013 ASME manufacturing science and engineering conference (MSEC 2013), Madison, Wisconsin
24. Okamura AM, Simone C, O'Leary MD (2004) Force modeling for needle insertion into soft tissue. IEEE Trans Biomed Eng 51:1707–1716
25. Wang YC, Chen RK, Bruce LT, Shih AJ (2014) Advanced five-plane lancet needle design, grinding, and tissue insertion. In: 2014 ASME manufacturing science and engineering conference (MSEC 2014), Detroit, Michigan